NON-LINEAR STRUCTURE FORMATION IN COSMOLOGIES WITH EARLY DARK ENERGY

M   B   [1], M   D   [2] C   W   [2]
[1] Z   ¨ A   , U   ¨ H   , A   -Ü -S . 2, 69120 H   , G
[2] I   ¨ T   P   , U   ¨ H   , P   16, 69120 H   , G

ABSTRACT

We argue that a few per cent of "Early Dark Energy" can be detected by the statistics of nonlinear structures. The presence of Dark Energy during linear structure formation is natural in models where the present tiny Dark-Energy density is related to the age of the Universe rather than a new fundamental small parameter. Generalisation of the spherical collapse model shows that the linear collapse parameter δ_c is *lowered*. The corresponding relative enhancement of weak gravitational lensing on arc-minute scales lowers the value of σ_8 inferred from a given lensing amplitude as compared to ΛCDM. In presence of Early Dark Energy, structures grow slower, such that for given σ_8 the number of galaxies and galaxy clusters is substantially increased at moderate and high redshift. For realistic models, the number of clusters detectable through their thermal Sunyaev-Zel'dovich effect at redshift unity and above, e.g. with the *Planck* satellite, can be an order of magnitude larger than for ΛCDM.

1. I

According to observations of Supernovae Ia (SNe Ia) (Riess et al., 2004), the Cosmic Microwave Background (CMB) (Spergel et al., 2003; Readhead et al., 2004; Goldstein et al., 2003; Rebolo et al., 2004) and Large Scale Structure (LSS) (Tegmark et al., 2004; Hawkins et al., 2003), the expansion of our Universe is accelerating today. A plausible candidate to drive such an acceleration is Dark Energy which may be described by an (effective, Doran & Jäckel 2002) scalar field (Wetterich, 1988; Ratra & Peebles, 1988; Caldwell et al., 1998; Caldwell, 2002). Such scalar field models have been shown to admit attractor solutions (Wetterich, 1988; Ratra & Peebles, 1988; Liddle & Scherrer, 1999; Zlatev & Steinhardt, 1999) where the Dark Energy component "tracks" the dominant component of the cosmological fluid. It is therefore natural to assume that Dark Energy might be non-negligible during extended periods of the evolution of our Universe.

For a mildly varying Dark Energy fraction during the whole history of the Universe, the present tiny Dark-Energy density can be linked to the huge age of the Universe. Such an "Early Dark Energy" contribution has been shown to influence the CMB (Doran et al., 2001a; Caldwell et al., 2003) and linear structure growth (Ferreira & Joyce, 1998; Doran et al., 2001b). From the CMB and LSS data, one infers a current limit on the Dark Energy contribution Ω_d during recombination and structure formation of $\Omega_d \lesssim 10\%$. Intriguingly, the effect of Early Dark Energy on structure formation is particularly strong, because it influences the entire structure formation period in contrast to a cosmological constant model or any other model of Dark Energy with $\Omega_d \to 0$ at earlier times.

The non-linear structure growth in Dark Energy scenarios has been subject of several investigations (see e.g. Wang & Steinhardt 1998; Ma et al. 1999; Linder & Jenkins 2003). In contrast to this work, we will focus on the implications of an Early Dark Energy component. This has two major effects. First, Early Dark Energy lowers the *linear* growth rate for structures. As a consequence, for a given present amplitude σ_8, the amplitude of structures at high redshift is higher as compared to ΛCDM. Second, on the *non-linear* level, there is more structure than one would naively expect from the linear amplitude in ΛCDM. In consequence, the abundance of collapsed objects is considerably higher at redshifts $z \sim 1$ than in a standard ΛCDM

universe. The decisive quantity for the number of non-linear objects is the probability for a region containing massive particles with a total mass M to collapse at a redshift z_c. It is proportional to

$$\exp\left[-\frac{\delta_i^2}{2\sigma_{i,R}^2}\right] , \qquad (1)$$

where the density contrast at early times (e.g. at matter-radiation equality), δ_i, is chosen such that the region collapses by redshift z_c, and the variance at early times, $\sigma_{i,R}$, is evaluated on a linear scale corresponding to the mass, $R \propto (M/\rho)^{1/3}$. For a given present fluctuation amplitude σ_8, the value of $\sigma_{i,R}$ is larger in cosmologies with Early Dark Energy as compared to ΛCDM. Since δ_i depends only mildly on the detailed cosmology, this enhancement of σ_i explains the enhancement of non-linear structures relative to ΛCDM. Conversely, the value of σ_8 required to explain the number counts of non-linear objects or weak gravitational lensing on small angular scales is smaller for models with Early Dark Energy than for ΛCDM. Comparison of the linear fluctuation amplitude (e.g. from galaxy correlations or weak gravitational lensing on large angular scales) with the power in non-linear structures could thus provide clear evidence for the presence of Early Dark Energy.

The crucial quantity for Early Dark Energy is its average density fraction during structure formation, $\Omega_{d,sf}$ (see Doran et al. 2001b for a precise definition). As an example for the high sensitivity of non-linear structures to $\Omega_{d,sf}$, we present two models with $\Omega_{d,sf} = 0.04$. We should also mention that a possible coupling between Dark Energy and Dark Matter could modify our results, but will be neglected in this work.

We use a particularly simple and direct parametrisation of the Dark Energy evolution (Wetterich, 2004). The parameters are the amount of Dark Energy today $\Omega_{d,0}$, the equation-of-state parameter today w_0, and the amount of Dark Energy at early times $\Omega_{d,e}$ to which it asymptotes for $z \to \infty$. One important feature of our parametrisation is a non-vanishing Dark-Energy contribution during recombination and structure formation. For illustration, we pick two models at random from a Monte-Carlo chain. We select models for which σ_8 is close to 0.8, the optical depth $\tau < 0.2$ and the spectral index of initial scalar perturbations is $n = 0.99$ and $n = 1.05$ respectively. The data we use for the Monte-Carlo chains are CMB (Spergel et al., 2003; Readhead et al., 2004; Goldstein et al.,

2003; Rebolo et al., 2004) and LSS data (Tegmark et al., 2004) and SNe Ia (Riess et al., 2004), thus both models describe current observations well. The parameters for model (I) are: $\Omega_{m,0}h^2 = 0.146$, $\Omega_b h^2 = 0.026$, $h = 0.67$, $n = 1.05$, $\tau = 0.18$, $w_0 = -0.93$ and $\Omega_{d,e} = 2 \times 10^{-4}$, leading to an effective Dark Energy contribution during structure formation (Doran et al., 2001b) of $\Omega_{d,sf} = 0.04$ and $\sigma_8 = 0.82$. Model (II) is given by $\Omega_{m,0}h^2 = 0.140$, $\Omega_{b,0}h^2 = 0.023$, $h = 0.62$, $n = 0.99$, $\tau = 0.18$, $w_0 = -0.99$ and $\Omega_{d,e} = 8 \times 10^{-4}$, leading to $\Omega_{d,sf} = 0.04$ and $\sigma_8 = 0.78$. We compare these models to ΛCDM with $\Omega_{m,0} = 0.3$, $\Omega_{\Lambda,0} = 0.7$, $h = 0.65$ and $\sigma_8 = 0.84$.

2. S   E   D   E

2.1. Solutions for early times

The qualitative features of the effects of Early Dark Energy can be understood analytically within the spherical collapse model. We consider a homogeneous, spherical overdensity which expands, reaches its maximum radius ("turn-around") at a scale factor a_{ta} and then collapses to reach virial equilibrium. We restrict the consideration to the matter-dominated era, i.e. we neglect the very slow growth of a perturbation inside the horizon during the radiation-dominated era.

Following Wang & Steinhardt (1998), we refer all quantities to their values at turn-around. Let ω and λ be the density parameters, at turn-around, of the (Dark) Matter and the Dark Energy, respectively. The cosmological scale factor x and the radius y of the density perturbation are normalised to unity at turn-around,

$$x \equiv \frac{a}{a_{ta}}, \quad y \equiv \frac{R}{R_{ta}}. \tag{2}$$

The spherical collapse of the perturbation is then described by the two Friedmann equations

$$\dot{x} = \left[\frac{\omega}{x} + \lambda x^2 g(x) + (1 - \omega - \lambda)\right]^{1/2}, \tag{3}$$

$$\ddot{y} = -\frac{\omega \zeta}{2y^2} - \frac{1 + 3w(x)}{2}\lambda g(x) y, \tag{4}$$

where dots denote derivatives with respect to the dimension-less time parameter

$$\tau \equiv H_{ta} t. \tag{5}$$

The parameter ζ quantifies the matter overdensity at turn-around in a spherical volume which will collapse at a later, pre-defined time. It is determined by solving (4) with the boundary conditions $y = 0$ at $\tau = 0$ and $\dot{y} = 0$ at turn-around, and requiring that $y = 1$ at turn-around. In other words, once the collapse time (or redshift) is fixed when the perturbation formally collapses to zero radius, ζ is chosen such that the maximum radius is reached at the turn-around time, given the boundary conditions. The function $g(x)$ quantifies the change in the Dark-Energy density with x relative to turn-around,

$$g(x) = \exp\left[-3\int_1^x [1 + w(x')]\mathrm{d}\ln x'\right] \equiv x^{-3(1+\bar{w})}, \tag{6}$$

where $\bar{w}$ is a suitably averaged equation-of-state parameter. For constant w, one has $\bar{w} = w$, but in general w and $\bar{w}$ are functions of τ or, equivalently, x.

We assume that the Dark-Energy density is always sufficiently smaller than the matter density at early times, i.e.

$$g(x) \ll x^{-3}, \quad x^3 g(x) \ll 1 \quad \text{for} \quad x \to 0. \tag{7}$$

Then, from (3),

$$\mathrm{d}\tau \approx \sqrt{\frac{x}{\omega}}\left(1 - \frac{1 - \omega - \lambda}{2\omega}x\right)\mathrm{d}x \tag{8}$$

for $x \ll 1$, and thus, at early times,

$$\sqrt{\omega}\tau \approx \frac{2}{3}x^{3/2}\left[1 - \frac{3}{10}\frac{1 - \omega - \lambda}{\omega}x\right], \tag{9}$$

without any effect of Dark Energy to second order in x.

Upon multiplication with $2\dot{y}$, Eq. (4) becomes

$$\frac{\mathrm{d}(\dot{y}^2)}{\mathrm{d}\tau} = \omega\zeta\frac{\mathrm{d}(1/y)}{\mathrm{d}\tau} - \frac{1 + 3w}{2}\lambda g(x)\frac{\mathrm{d}(y^2)}{\mathrm{d}\tau}. \tag{10}$$

Integration gives

$$\dot{y}^2 = \frac{\omega\zeta}{y} - \lambda\int_0^y [1 + 3w(x')]g(x')y'\mathrm{d}y' + C, \tag{11}$$

with the integration constant C set by the requirement at turn-around that

$$\dot{y}|_{y=1} = 0, \tag{12}$$

which is satisfied if

$$C = \lambda\int_0^1 [1 + 3w(x')]g(x')y'\mathrm{d}y' - \omega\zeta. \tag{13}$$

When inserted back into (11), this yields

$$\dot{y}^2 = \omega\zeta\left(\frac{1}{y} - 1\right) + \lambda\int_y^1 [1 + 3w(x')]g(x')y'\mathrm{d}y'. \tag{14}$$

We will have to study (14) at very early times, i.e. for $x \to 0$ and $y \to 0$. In that limit, the integral (14) will either converge or diverge as x and y approach zero. Suppose the integral converges,

$$\lim_{y\to 0}\int_y^1 (1 + 3w)g(x)y\mathrm{d}y \equiv I < \infty. \tag{15}$$

Then, for $y \to 0$, Eq. (14) can be approximated by

$$\frac{\sqrt{y}\mathrm{d}y}{\sqrt{1 - Ay}} = \sqrt{\omega\zeta}\mathrm{d}\tau, \quad A \equiv 1 - \frac{\lambda I}{\omega\zeta}, \tag{16}$$

which can be integrated after expanding the denominator into a Taylor series,

$$\sqrt{\omega\zeta}\tau \approx \int_0^y \sqrt{y}\left(1 + \frac{Ay}{2}\right) = \frac{2}{3}y^{3/2}\left(1 + \frac{3A}{10}y\right). \tag{17}$$

For example, if the Dark Energy is described by a cosmological constant, $w = -1$ and $g(x) = 1$, thus $I = -1$ and $A = 1 + \lambda/\omega\zeta$.

The integral I defined in (15) will diverge if $g(x)$ increases steeply as $x \to 0$. Then, it will be dominated by the behaviour of its integrand for $x \to 0$. Let

$$\lim_{x\to 0} w(x) \equiv w_{ini}, \quad \lim_{x\to 0} g(x) \equiv \gamma x^{-3(1+w_{ini})} \tag{18}$$

with a constant $\gamma \ll 1$, and we further assume y to be proportional to x at early times, $y = \alpha x$, which will be justified in hindsight. Then,

$$\begin{aligned} I &\approx (1 + 3w_{ini})\,\alpha^2\gamma\lim_{x\to 0}\int_x^1 x'^{-3(1+w_{ini})}\,x'\mathrm{d}x' \\ &\approx \alpha^2\gamma\lim_{x\to 0}\left(x'^{-1-3w_{ini}}\big|_x^1\right) \\ &\approx \frac{\gamma\alpha^{3(1+w_{ini})}}{y^{1+3w_{ini}}}. \end{aligned} \tag{19}$$

I is thus expected to diverge if $w_{\text{ini}} \geq -1/3$. With (14), this yields for early times

$$\dot{y} = \left[\frac{\omega\zeta}{y} - \omega\zeta + \lambda\gamma \frac{\alpha^{3(1+w_{\text{ini}})}}{y^{1+3w_{\text{ini}}}} \right]^{1/2} . \qquad (20)$$

According to (7), $w_{\text{ini}} \leq 0$, because otherwise the Dark-Energy density would grow above the matter density. Let $w_{\text{ini}} = 0$ first, then (20) implies

$$\begin{aligned}
\dot{y} &= \left[\frac{\omega\zeta + \lambda\gamma\alpha^3}{y} - \omega\zeta \right]^{1/2} \\
&\approx \sqrt{\frac{\omega\zeta + \lambda\gamma\alpha^3}{y}} \left(1 - \frac{\omega\zeta}{2(\omega\zeta + \lambda\gamma\alpha^3)} y \right) , \qquad (21)
\end{aligned}$$

which can be integrated to give

$$\sqrt{\omega\zeta}\tau \approx \frac{2}{3} y^{3/2} \sqrt{B} \left(1 + \frac{3}{10} By \right) , \quad B \equiv \frac{\omega\zeta}{\omega\zeta + \lambda\gamma\alpha^3} . \qquad (22)$$

If $-1/3 < w_{\text{ini}} < 0$, we can replace B by

$$B = \frac{\omega\zeta}{\omega\zeta + \lambda\gamma\alpha^{3(1+w_{\text{ini}})}y^{-3w_{\text{ini}}}} \approx 1 - \frac{\lambda\gamma}{\omega\zeta}\alpha^{3(1+w_{\text{ini}})}y^{-3w_{\text{ini}}} \qquad (23)$$

to account for the gentle change in the coefficient B with y.

Equating $\sqrt{\zeta}$ times (9) to (17) and squaring yields

$$\zeta x^3 \left(1 - \frac{3}{5}\frac{1-\omega-\lambda}{\omega}x \right) \approx y^3 \left(1 + \frac{3A}{5}y \right) , \qquad (24)$$

while the same procedure applied to (22) implies

$$\zeta x^3 \left(1 - \frac{3}{5}\frac{1-\omega-\lambda}{\omega}x \right) \approx y^3 B \left(1 + \frac{3B}{5}y \right) . \qquad (25)$$

Now, $B \approx 1$ to lowest order because $\gamma \ll 1$ and $y \ll 1$ at early times, thus

$$y \approx \zeta^{1/3} x , \quad \alpha = \zeta^{1/3} \qquad (26)$$

to lowest order, and the earlier assumption $y \approx \alpha x$ is verified. The definition of B in (22) and (23) then simplifies to

$$B \approx 1 - \frac{\lambda\gamma\zeta^{w_{\text{ini}}}y^{-3w_{\text{ini}}}}{\omega} \qquad (27)$$

In order to illustrate the procedure described above, let us assume $w(a) = -a$, or $w(x) = -a_{\text{ta}}x$, for which $g(x)$ from (6) becomes

$$g(x) = \exp\left[-3 \int_1^x (1 - a_{\text{ta}}x')\, d\ln x' \right] = \frac{e^{3a_{\text{ta}}(x-1)}}{x^3} . \qquad (28)$$

This yields

$$\begin{aligned}
\int_y^1 [1 + 3w(x')]\, g(x')\, y'\mathrm{d}y' &\approx \alpha^2 \left[\frac{e^{3a_{\text{ta}}(x-1)}}{x} - 1 \right] \\
&\approx \frac{\alpha^2 e^{-3a_{\text{ta}}}}{x} \approx \frac{\alpha^3 e^{-3a_{\text{ta}}}}{y} . \qquad (29)
\end{aligned}$$

Following (18), we have

$$w_{\text{ini}} = 0 , \quad \gamma = e^{-3a_{\text{ta}}} , \qquad (30)$$

confirming that $\gamma \ll 1$ for typical values of $a_{\text{ta}} \lesssim 1$. Thus, (29) agrees with the more general result (19).

2.2. Overdensity and linear density contrast

Since the background matter density changes in proportion to x^{-3}, while the matter density inside the perturbation is proportional to y^{-3}, the overdensity inside the perturbation obeys

$$\Delta = \frac{\zeta x^3}{y^3} , \qquad (31)$$

which, according to (24) and (25), is

$$\Delta \approx \begin{cases} 1 + \dfrac{3A}{5}y + \dfrac{3}{5}\dfrac{1-\omega-\lambda}{\omega}x & \text{for} \quad w_{\text{ini}} < -1/3 \\[2mm] 1 + \dfrac{3B}{5}y + \dfrac{3}{5}\dfrac{1-\omega-\lambda}{\omega}x & \text{else} \end{cases} \qquad (32)$$

at early times. The two solutions join at $w_{\text{ini}} = -1/3$, as they should. For $w_{\text{ini}} = -1/3$, $I = 0$ because $(1 + 3w_{\text{ini}}) = 0$ in Eq. (19), thus $B = 1$. Also, $A \to 1$ for $w \to -1/3$ according to (15) and (16).

The overdensity Δ_v within virialised objects should only very weakly be affected by the (Early) Dark Energy because Dark Matter dominates the virialisation process. We verify this as described in Appendix A..

The *linear* density *contrast* δ can be used to relate the non-linear overdensity Δ with the density that would result from linear evolution of the same initial perturbation within linear evolution. With the growth factor $D_+(x)$ at a given time or normalised scale factor x one has at the collapse time $x_c > 1$

$$\delta_c = \lim_{x\to 0} \left[\frac{D_+(x_c)}{D_+(x)} [\Delta(x) - 1] \right] , \qquad (33)$$

The linear density contrast at collapse time δ_c is a crucial ingredient for the Press-Schechter and related mass functions (Press & Schechter, 1974; Sheth & Tormen, 1999). We shall explain below why δ_c is substantially smaller for Early Dark-Energy models as compared to ΛCDM. This finding is a central ingredient for our results.

2.3. Results for δ_c

We show in Fig. 1 the linear critical overdensity δ_c as a function of z_c. While the results range around $\delta_c = 3/5(3\pi/2)^{2/3} \approx 1.686$ for ΛCDM and OCDM, quite independent of the collapse redshift, they fall below for the Early-DE models, dropping even to $\delta_c \approx 1.4$ for $z_c = 0$.

We return to (33) in order to understand why δ_c is lower for Early-DE than for, e.g., the ΛCDM model. It turns out numerically that the overdensity $(\Delta - 1)$ is not changed much in the Early-DE compared to the ΛCDM model. For a collapse redshift of $z_c = 0$, for instance, $(\Delta - 1)/x$ is lower by only 4% in the Early-DE than in the ΛCDM model. The main difference, however, is caused by the growth-factor ratio in (33), as shown in Fig. 2.

The curves show the growth factor divided by the scale factor, $D_+(a)/a$, as a function of a, for one of the Early-DE models and for ΛCDM. Both lower curves are normalised such that they start from unity at early times, as it should be according to (33). Obviously, the linear growth in Early-DE falls behind that in ΛCDM, starting from an overdensity of the same amplitude. The reason is that the expansion rate in the Early-DE models is higher at early times than in ΛCDM, which increases the friction term $(\dot{a}/a)$ in the equation

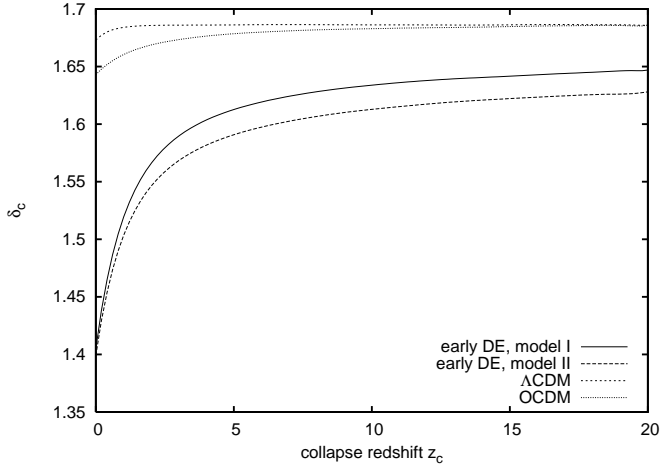$$\ddot{\delta} + 2\frac{\dot{a}}{a}\dot{\delta} - 4\pi G\rho\delta = 0 \qquad (34)$$

FIG. 1.—The linear density contrast at collapse, δ_c is plotted as a function of the collapse redshift z_c for two models with early Dark Energy, and for ΛCDM and OCDM for comparison. While the ΛCDM and the OCDM models show very similar behaviour, with δ_c near the "canonical" value of 1.686, the Early-DE models fall substantially below, in particular for low collapse redshifts.

FIG. 2.—The linear growth factor divided by the scale factor, $D_+(a)/a$, is shown here as a function of a for an Early-DE model, a model with constant $w = -0.8$, and for the ΛCDM model. The lower curves are normalised to unity at early times, i.e. they illustrate the growth of perturbations starting from the same density contrast in the two cosmologies. The upper curves are normalised to unity at present ($a = 1$), illustrating the growth of structures reaching the same level today in both cosmologies. Starting from the same amplitude, the growth in the Early-DE model falls behind that in ΛCDM, largely causing the reduction in the overdensity parameter δ_c. Structures have to grow earlier in Early-DE models than in ΛCDM to reach the same fluctuation amplitude today.

governing the growth factor. As we shall see below, the reduced linear overdensity δ_c expected in Early-DE models has pronounced consequences for nonlinear structure formation.

The two upper curves in Fig. 2 show the growth factor normalised to unity at present, i.e. reflecting the evolution back in time of structures reaching the same amplitude today. They show that structures need to grow earlier in Early-DE models than in ΛCDM models to reach the same level at the present time.

3. C

3.1. Distances and age

The influence of Early Dark Energy on global geometrical properties of the Universe is illustrated in Fig. 3, which shows the angular-diameter distance $D_{ang}(z)$ in units of cH_0^{-1} as a function of redshift relative to ΛCDM. A model with constant $w = -0.8$ is shown for comparison. Note that this curve also gives the ratio of luminosity distances $D_{lum}(z)$ between Dark-Energy models and ΛCDM because $D_{lum}(z)$ and $D_{ang}(z)$ only differ by the ratio of scale factors between emission and observation.

As the figure shows, distance measures are changed only moderately, by $\lesssim 8\%$ for source redshifts below $z = 2$. The cosmic time is changed by a larger amount, as can be seen in Fig. 4. It shows the cosmic time as a function of redshift in units of H_0^{-1}, again relative to ΛCDM.

The increased expansion rate of the Universe compared to ΛCDM, in particular at early times, reduces the age of the Universe by approximately $(5 - 10)\%$ at low redshifts. The effect of Dark Energy with constant $w = -0.8$ is substantially less pronounced.

3.2. The mass function

The reduced linear density contrast δ_c necessary for spherical collapse has a pronounced influence on the mass function of Dark-Matter halos. The Press-Schechter mass function for ex-
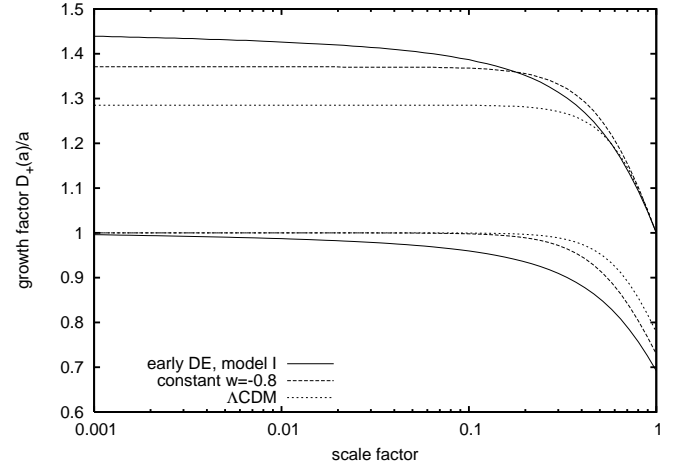
ample can be written as (Press & Schechter, 1974)

$$
\begin{aligned}
N(M, z)\mathrm{d}M &= \sqrt{\frac{2}{\pi}} \frac{\rho_0 \delta_c}{\sigma_R D_+(z)} \frac{\mathrm{d}\ln\sigma_R}{\mathrm{d}M} \\
&\times \exp\left(-\frac{\delta_c^2}{2\sigma_R^2 D_+^2(z)}\right) \frac{\mathrm{d}M}{M} ,
\end{aligned}
\qquad (35)
$$

showing that δ_c^2 is compared in the argument of the exponential function to the variance $\sigma_R^2 D_+^2(z)$ of the Dark-Matter density field smoothed on scales R corresponding to the mass M, with $D_+(z = 0) = 1$. Linear quantities occur in the exponential of the Press-Schechter mass function because it predicts the distribution of the later non-linear fluctuations from their linear distribution at early times. Even small reductions of δ_c, as they are illustrated in Fig. 1, lead to a noticeable increase in the mass function for a fixed normalisation parameter σ_8 of the Dark-Matter power spectrum. The increase of the mass function in the two Early Dark Energy models compared to ΛCDM is illustrated in Fig. 5.

The figure shows the mass function proposed by Sheth & Tormen (1999), which assumes ellipsoidal rather than spherical halo collapse and reproduces the halo abundances in simulations significantly better than the original Press-Schechter mass function. As Fig. 5 shows, Early Dark Energy has a pronounced effect on the mass function. While halos with masses $\lesssim 10^{13} h^{-1} M_\odot$ have approximately equal abundances as in ΛCDM, massive clusters with $M \gtrsim 5 \times 10^{14} h^{-1} M_\odot$ are of order $1.5 - 2.5$ times more abundant at the present epoch, provided the models are normalised according to the CMB temperature fluctuations. At redshift unity, however, the mass functions differ by a factors of $\sim (5 - 10)$ for massive clusters. Therefore, even if the models were normalised such as to get closer to the cluster abundance expected in ΛCDM today, they still predicted a higher number density of high-redshift clusters. As Fig. 7 shows in more detail, the normalisation parameter
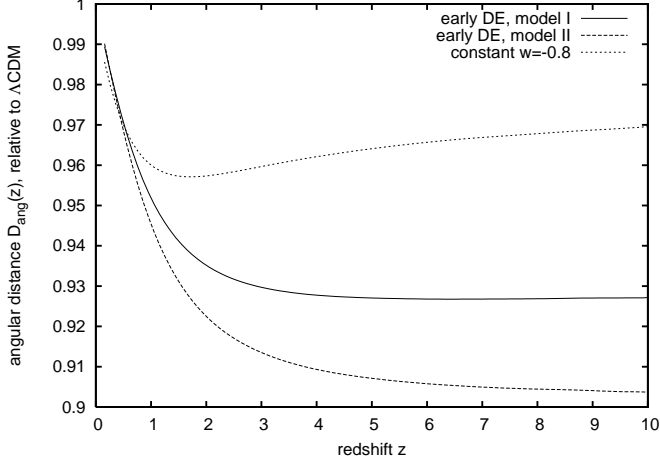
F . 3.—The angular-diameter distance as a function of redshift is shown for two Early-DE models relative to ΛCDM. A model with constant $w = -0.8$ is also shown for comparison.
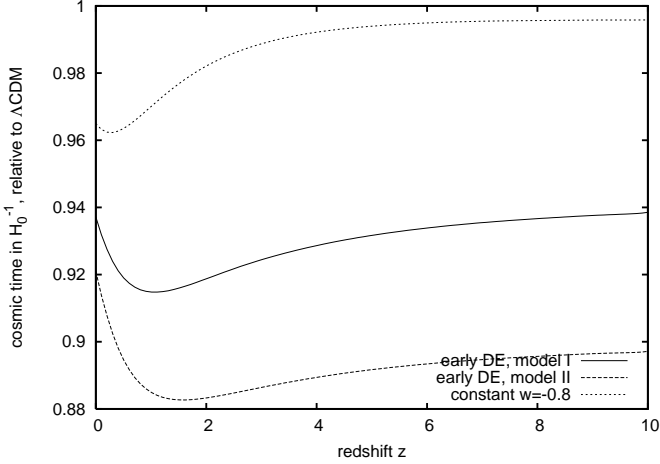
F . 4.—Cosmic time in units of H_0^{-1} as a function of redshift, relative to ΛCDM. Three curves are given, two for the Early-DE models and one for a constant $w = -0.8$ for comparison. For fixed Hubble constant H_0, Early Dark Energy makes the universe younger today by $(5 - 10)\%$ compared to ΛCDM, while a fixed present age would reduce H_0.

would have to be lowered to $\sigma_8 \approx 0.69$ for the Early-DE models to reproduce the halo abundance at $z = 0$ of a ΛCDM model with $\sigma = 0.84$.

The earlier development of the mass function naturally leads to enhanced dynamical activity of Dark-Matter halos, in particular at the highest cluster masses. The extended Press-Schechter formalism (Bond et al., 1991) allows the calculation of the merger probability,

$$\frac{\mathrm{d}^2 p}{\mathrm{d} \ln \Delta M \mathrm{d} t}(M, z) , \qquad (36)$$

i.e. the probability for a halo of mass M to merge within time t at redshift z with another halo of mass ΔM (Lacey & Cole, 1993, 1994). Multiplying (36) with the mass function and the differential cosmic volume $\mathrm{d}V$ corresponding to a redshift interval $\mathrm{d}z$, and integrating over a mass range from M_1 to M_2 and over the time t corresponding to a redshift interval $z - \delta z$ to z yields the total number of mergers between a halo of mass M and another halo of mass between M_1 and M_2, within the time interval from
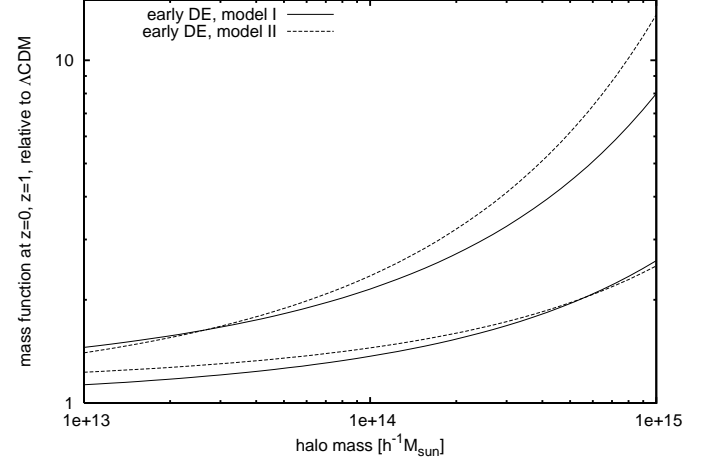
F . 5.—Ratio between the Dark-Matter halo mass function between 10^{13} and $10^{15} h^{-1} M_\odot$ in two Early-Dark Energy models compared to ΛCDM. Two pairs of curves are given, the lower for $z = 0$, the upper for $z = 1$. The ratio increases monotonically with increasing mass. While massive clusters today are $1.5 - 2.5$ times more abundant in CMB-normalised Early-DE compared to the ΛCDM model, their number is expected to be up to an order of magnitude higher at redshift $z = 1$ in Early-DE models.

$t(z + \delta z)$ and $t(z)$,

$$
\begin{aligned}
\delta N(M, z) &= N(M, z) \left| \frac{\mathrm{d}V}{\mathrm{d}z} \right| \int_{\ln M_1}^{\ln M_2} \mathrm{d} \ln M \\
&\times \int_{t(z+\delta z)}^{t(z)} \mathrm{d}t \frac{\mathrm{d}^2 p(M, z)}{\mathrm{d} \ln M \mathrm{d}t} .
\end{aligned} \qquad (37)
$$

We set $M = 5 \times 10^{14} h^{-1} M_\odot$, $M_1 = M/4$, $M_2 = M$, and $\delta z = 0.2$. In other words, we compute using expression (37) the number per unit redshift of cluster-sized Dark-Matter halos at redshift z that have undergone a major merger within z and $z+0.2$. Figure 6 shows the ratio between the merger number in the two Early-DE models relative to ΛCDM.

The two curves in the figure show that major mergers at moderate and high redshifts of cluster-sized halos are substantially more frequent in the two Early Dark-Energy models compared to ΛCDM. This reflects our previous result that the halo mass function grows earlier in the Early-DE models, leading to enhanced merger activity at earlier times.

Of course, these results on the abundance of Dark-Matter halos depend sensitively on the normalisation of the power spectrum, as the rising curves in Fig. 7 illustrate. Much less dependent on the amplitude of the power spectrum is the expected ratio of halo numbers above two different redshifts. The falling curves in Fig. 7 give examples.

The curves show for three cosmological models in dependence of the normalisation parameter σ_8 by how much the number of cluster-sized halos with mass $M \geq 10^{14} h^{-1} M_\odot$ grows between redshifts unity and zero. For $\sigma_8 = 0.8$ in ΛCDM, there are about four times more clusters today than there were at redshift unity, and about two times more in the Early-DE models. This corroborates that clusters are more abundant at high redshifts in the Early-DE models compared to ΛCDM. Since CDM is a hierarchical model of structure formation, a similar effect appears for lower-mass halos at higher redshift. In the Early-DE models, for instance, the number of galaxy-sized halos evolves much less than in ΛCDM above redshifts 2 and beyond.
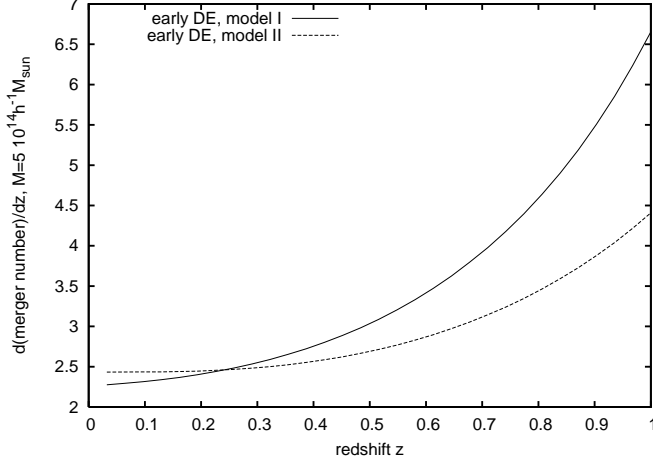
F .6.—The number per unit redshift of cluster-sized halos with mass $M = 5 \times 10^{14}\, h^{-1}\, M_\odot$ is shown here which have undergone a major merger with another halo of mass between $M/4$ and M within redshifts z and $z + 0.2$. Both curves are normalised to the merger number in ΛCDM. Reflecting the earlier growth of the mass function in Early-DE models compared to ΛCDM, major mergers of massive halos are about a factor of ≈ 5 more frequent at redshifts near unity.

F .7.—*Rising curves*: The number of halos per square degree with masses $M \geq 10^{14}\, h^{-1}\, M_\odot$ is shown as a function of the normalisation parameter σ_8. The upper and lower curves show the numbers of halos with redshifts $z \geq 0$ and $z \geq 1$, respectively. At $\sigma_8 \sim 0.7$, the Early-DE models have ~ 25 cluster-sized halos with $z \geq 0$ per square degree, for which the ΛCDM model needs $\sigma_8 \sim 0.9$. The *falling curves* show the ratios of halo numbers with mass $M \geq 10^{14}\, h^{-1}\, M_\odot$ above redshifts zero and unity for the two models of Early Dark Energy and for ΛCDM as a function of the normalisation parameter σ_8. At fixed $\sigma_8 \sim 0.8$, the number of cluster-sized halos grows by approximately twice as much in the ΛCDM compared to the Early-DE models.

3.3. Halo properties

Earlier work has found that Dark-Matter halos tend to be more concentrated if they form earlier, where the concentration c is the ratio between the halo's virial and scale radii (Navarro et al., 1997; Bullock et al., 2001; Eke et al., 2001). While the central slope of Dark-Matter density profiles in halos is still under some debate (cf. Power et al. (2003)), numerical simulations consistently show that halos in (Cold) Dark Matter have a steep density profile outside, and a flat density profile inside the scale radius. The definition of the virial radius changes in the literature, depending on whether the mean density enclosed by the virial radius is supposed to be 200 or another factor times the mean or the critical cosmic density. Different recipes have also been given for the statistical relation between the virial mass and the concentration of halos. They were tested against numerical results on Dark-Energy models by Dolag et al. (2004) who found that the algorithm described by Eke et al. (2001) worked for models with constant $w \neq -1$ without adaptation.

All algorithms have in common that they have to define a collapse redshift z_c for a halo of given mass M at redshift z, and a ratio between the central density of the halo and the mean or critical cosmic background density at z_c. Eke et al. (2001) define the collapse redshift by requiring that, at z_c, the amplitude of the power spectrum at the mass scale of the halo reaches a given fixed value. We show in Fig. 8 the expected concentration according to Eke et al.'s prescription as a function of halo mass at redshifts zero (upper curves) and unity (lower curves).

In agreement with earlier studies (Bartelmann et al., 2002; Klypin et al., 2003; Dolag et al., 2004; Weinberg & Kamionkowski, 2003), halos in cosmologies with dynamical Dark Energy tend to be more concentrated than in ΛCDM, reflecting their earlier growth on a cosmological background with higher mean density. For galaxy-sized halos in the Early-DE models, the concentration increases by $\approx 20\%$ at redshift zero.
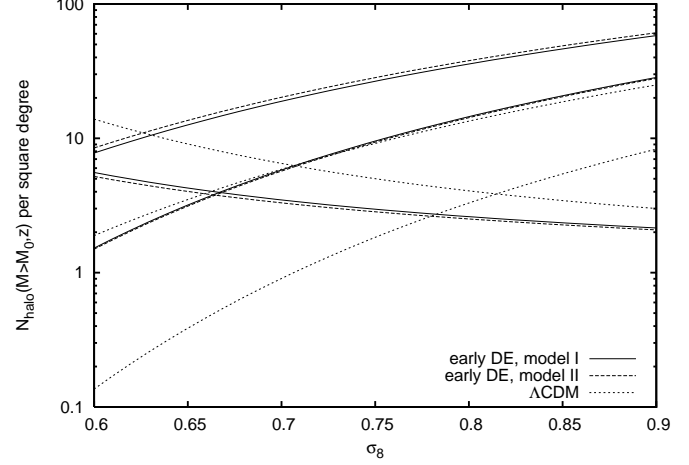
3.4. Gravitational lensing

The efficiency of gravitational lensing by isolated lenses such as galaxies or galaxy clusters is given by the critical surface-mass density

$$\Sigma_{\mathrm{cr}} = \frac{c^2}{4\pi G} \frac{D_{\mathrm{s}}}{D_{\mathrm{l}} D_{\mathrm{ls}}} \ , \qquad (38)$$

which contains the angular-diameter distances $D_{\mathrm{l,s,ls}}$ from the observer to the lens, the source, and from the lens to the source, respectively (e.g. Schneider et al. (1992)). The effective lensing distance $D_{\mathrm{eff}} \equiv D_{\mathrm{l}} D_{\mathrm{ls}} / D_{\mathrm{s}}$ thus measures the geometrical efficiency of a given mass distribution.

Dark Energy reduces the effective lensing distance compared to ΛCDM. For sources at redshift $z_{\mathrm{s}} = 2$, as assumed for the figure, identical mass distributions are $\approx 5\%$ less efficient at $z_{\mathrm{l}} \approx 0.4$, and $\approx 10\%$ less efficient at $z_{\mathrm{l}} \approx 1.0$, in Early-DE than in ΛCDM models. Compared to the increased concentration of the Dark-Matter halos, this effect is less important for strong lensing by galaxies, groups or clusters (Meneghetti et al., 2004).

In sufficient approximation, weak gravitational lensing by large-scale structures can be described by the power spectrum $P_\kappa(l)$ of the effective convergence κ (see Bartelmann & Schneider (2001) for a review). Earlier structure growth also affects P_κ, as shown in Fig. 10.

The weak-lensing power is illustrated there plotting $l^2 P_\kappa(l)$ as a function of angular scale for the two Early-DE models, relative to the ΛCDM model. Two pairs of curves are given for the two source redshifts $z_{\mathrm{s}} = 1$ and 1.5. The curves tend to unity at angular scales above 10 arc minutes, indicating that weak lensing will not be modified compared to ΛCDM on large angular scales. On small angular scales $\lesssim 1'$ however, the weak-lensing power in the Early-DE models exceeds that in the ΛCDM model by $\sim 40\%$ for $z_{\mathrm{s}} = 1$ and by $\sim 55\%$ for $z_{\mathrm{s}} = 1.5$. This would imply that σ_8 as derived from weak-lensing measurements could be $\sim 1.4^{-1/2} \approx 0.8$ times smaller than inferred assuming a ΛCDM model.
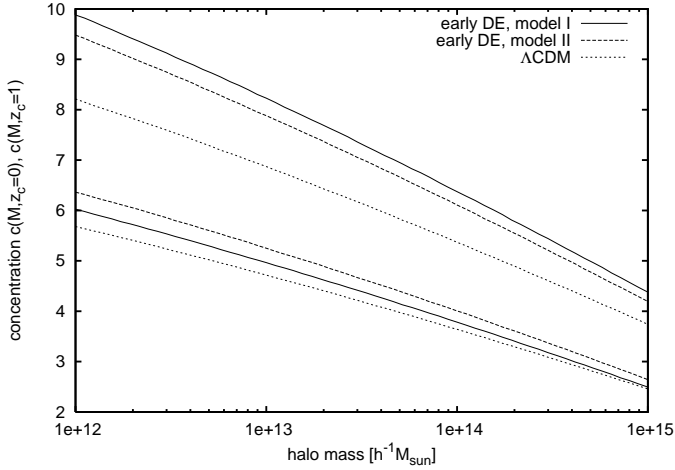
FIG. 8.—Halo concentrations as functions of mass, according to Eke et al.'s algorithm, for redshifts unity (lower curves) and zero (upper curves). Results for the two Early-DE models and for ΛCDM are given. Halos in Early-DE models are more concentrated than in ΛCDM, and the difference increases for smaller masses.
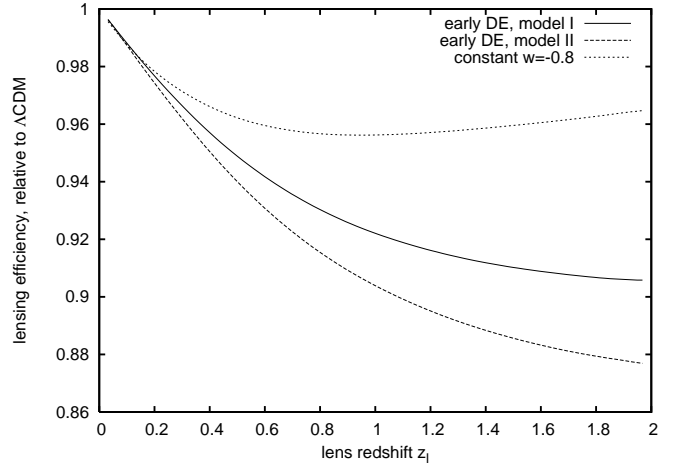
FIG. 9.—The effective lensing distance is plotted here for the two Early-DE models, normalised by the result in ΛCDM. The curve for constant $w = -0.8$ is shown for comparison. Sources are assumed at redshift $z_s = 2$. The effective lensing distance is lower by $\approx 5\%$ in Early-DE than in ΛCDM models at typical lens redshifts near $z = 0.4$, and by $\lesssim 10\%$ at redshifts near unity.

3.5. Number counts of thermal Sunyaev-Zel'dovich clusters

The most significant observable consequence of Early-DE models identified so far is that the counts of cluster-sized halos should decrease significantly more slowly than in ΛCDM (cf. Figs. 5 and 7). While statistically complete galaxy-cluster samples are notoriously hard to identify, future cluster surveys based on the thermal Sunyaev-Zel'dovich (SZ) effect (Sunyaev & Zeldovich, 1972) should provide ideally suitable data for testing this prediction of Early-DE models.

The upcoming *Planck* satellite, due for launch in 2007, will observe the entire microwave sky in frequency bands between 30 and 857 GHz with an angular resolution of down to 5 arc minutes. One of its frequency bands is centred on 217 GHz where the (non-relativistic) thermal Sunyaev-Zel'dovich effect vanishes. *Planck*'s frequency bands are thus well-placed for identifying the unique spectral signature of the thermal SZ effect which reduces the CMB intensity below, and increases it above, 217 GHz. *Planck*'s high sensitivity and comparatively high angular resolution will enable it to detect a huge sample of clusters reaching high redshift.

Analytic estimates raise the expectation that *Planck* may find of order 30,000 galaxy clusters on the full sky (da Silva et al., 2000; Bartelmann et al., 2003), while simulations taking realistic foreground contamination, noise patterns and full-sky, multi-band filtering techniques into account arrive at lower numbers, $\lesssim 10,000$ (Schäfer et al., 2004). Nonetheless, the cluster sample expected from *Planck* will be enormous. Following the analytic description of the *Planck* cluster sample given in Bartelmann et al. (2003), we show in Fig. 11 the cumulative redshift distribution of clusters in the sample expected from *Planck* in the Early-DE models, normalised by the expectation in the ΛCDM model.

While the total number of detections is moderately increased by a factor of two to three, the number of high-redshift clusters detectable in Early-DE models is substantially higher than in ΛCDM. The number of clusters above redshift unity is already an order of magnitude larger. Thus, the number of clusters detected by *Planck* will provide a highly sensitive test for Early-DE compared to ΛCDM models.

Interestingly, observations of the CMB on small angular scales ($\lesssim 5'$) with the *Cosmic Background Imager* (CBI) indicate

a much higher temperature fluctuation amplitude than expected in ΛCDM with the normalisation $\sigma_8 \sim 0.8$ typically inferred from other observations (Padin et al., 2001; Mason et al., 2003). If due to the thermal SZ effect, these measurements require $\sigma_8 \gtrsim 1$ in the ΛCDM model (Bond et al., 2005), which would stretch other normalisation constraints to their limits. Cosmological models with Early Dark Energy such as those used here as examples could naturally explain this "CBI anomaly".

4. SUMMARY AND CONCLUSIONS

We have investigated expectations for the growth of non-linear structures in a model universe with Early Dark Energy. Such models assume that the accelerated cosmic expansion is driven by a scalar field which has non-negligible energy density all through cosmic history. We have selected two examples for such models with Early Dark Energy whose parameters are chosen such as to comply with the temperature fluctuations measured in the cosmic microwave background.

We have generalised the spherical-collapse model such that Dark Energy with variable equation-of-state parameter w can be taken into account. In our models the Dark Energy follows for $z \gtrsim 1$ the density of the dominant component in the mixture of cosmic fluids. Modified in this way, the spherical collapse model predicts that the linear density contrast necessary for collapse, δ_c, is lowered compared to ΛCDM models or Dark-Energy models with constant w.

This first result, which may appear unexpected, can be understood as follows. The requirement of having virialised halos at a given redshift sets the initial overdensity inside the spherical perturbation idealising the later halo. Early Dark Energy reduces the linear growth factor compared to ΛCDM due to its higher expansion rate in the young universe. The initial overdensity required for later collapse is thus extrapolated to lower linear overdensity at collapse time. Lower linear density contrast is thus sufficient for non-linear collapse, which increases the number of fluctuations capable of forming halos.

The effects of Early Dark Energy on the geometrical properties of the Universe are moderate. Assuming the same Hubble constant today, such models are $\sim 5\%$ younger than comparable ΛCDM models today, and the angular-diameter distances are
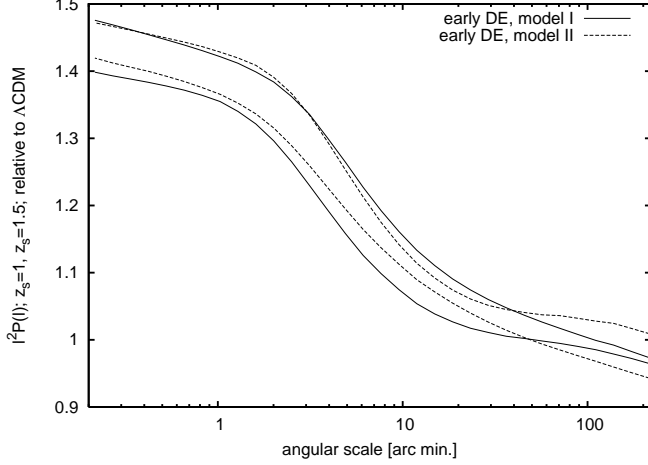
F 10.—The weak-lensing power, expressed by means of the convergence power spectrum as $l^2 P_\kappa(l)$, is plotted as a function of angular scale for the two Early-DE models for the two different source redshifts $z_s = 1$ and 1.5. The curves are normalised by the expectation in ΛCDM.

F 11.—*Falling curves*: Cumulative redshift distribution of clusters expected to be detected through their thermal Sunyaev-Zel'dovich effect by the *Planck* satellite. Curves are shown for the two models of Early Dark Energy and for ΛCDM, and they are normalised to show the number of clusters per 10 square degrees. Thermal-SZ cluster counts in the Early-DE models start at $z = 0$ at approximately twice the value in ΛCDM and reach to substantially higher redshifts. The *rising curves* show the redshift distributions in the Early-DE models, divided by the expectation in the ΛCDM model. For $z \geq 0$, the total number of detections should increase by a factor of 2–3, while the number of clusters at redshifts ≥ 1 should be about an order of magnitude higher in Early-DE compared to ΛCDM models.

lowered by no more than $\sim 10\%$ even to high redshifts. Yet, these effects are noticeably stronger than in Dark-Energy models with constant w; typically, they are roughly twice as large than in a model universe which has $w = -0.8$.

Since halos tend to grow earlier in Dark-Energy compared to ΛCDM models, their core densities are higher, and so are their concentration parameters. Using the prescription of Eke et al. for computing expected halo concentrations, we found that halos at redshift zero are more concentrated than in ΛCDM by $\sim 20\%$ for galaxy masses, and by $\sim 15\%$ for cluster masses. This increase is visible, but smaller for halos forming at higher redshift.

Strong gravitational lensing profits non-linearly from higher halo concentrations. On the other hand, the effective lensing distance (proportional to the inverse critical surface density for lensing) is lowered by Early Dark Energy, albeit weakly. At redshifts which are typical for strong-lensing galaxies or clusters, $\sim 0.3-0.8$, say, we found a reduction of the effective lensing distances of order $\sim 8\%$ compared to ΛCDM. The power of weak gravitational lensing by large-scale structures, however, is more substantially changed. While there is no difference in the weak-lensing power between Early Dark-Energy and ΛCDM models on large angular scales $\gtrsim 1°$, it is increased by $\sim 40\%$ on arc-minute scales for sources at redshift ~ 1. This implies a steeper increase with decreasing angular scale of, e.g. the two-point correlation function of the cosmic shear than expected in ΛCDM. It also implies that the normalisation of the Dark-Matter power spectrum, σ_8, inferred from weak lensing should be lowered by a factor of ~ 0.8 as compared to its value for a ΛCDM model.

The most pronounced effect, however, regards the present number density of massive halos and its evolution towards higher redshift. The Early Dark-Energy models we have studied here, normalised to the CMB temperature-fluctuation measurements, predict approximately the same number density of galaxy-sized halos today as expected in a ΛCDM universe, and a number density of cluster-sized halos which is $\sim 40\%$ higher. Given the uncertainties in cluster counts even at low redshift, this appears tolerable, although a very moderate reduction of σ_8 would establish complete agreement at redshift zero between the halo counts in Early Dark-Energy and ΛCDM models. However, this present cluster population shrinks much less quickly towards high redshift than in ΛCDM, implying that many more of the clusters existing today were already present at redshifts of
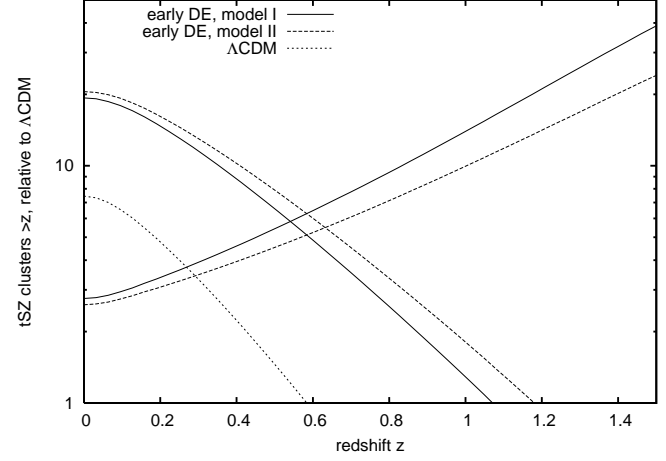
order unity.

The cluster population above a mass limit of $10^{14} h^{-1} M_\odot$ expected for $\sigma_8 = 0.8$ in Early Dark-Energy models shrinks by a factor of ~ 2.5 at redshift unity compared to redshift zero, but by a factor of ~ 4 in ΛCDM models. This discrepancy increases rapidly for more massive clusters. Raising the mass limit to $5 \times 10^{14} h^{-1} M_\odot$ makes the cluster population shrink by a factor of ~ 9 in the Early Dark-Energy models, but by a factor of ~ 28 in an equally-normalised ΛCDM model.

It appears reasonable here to distinguish two possibly different values of σ_8 extracted from linear and non-linear structure growth. As the mass function (35) shows, lowering δ_c due to Early Dark Energy can be compensated by equally lowering σ_8. This implies that approximately the same halo number at all redshifts as in the ΛCDM model can be reproduced in the Early Dark Energy models by suitably lowering σ_8. This σ_8 would then properly describe the abundance of non-linear, collapsed structures. This can be tested against the amplitude of linear structures, which is measurable for instance by the galaxy power spectrum on large scales or weak gravitational lensing on scales $\gtrsim 10'$. In other words, if the value of σ_8 extracted from non-linear structures within a ΛCDM model turns out systematically higher than the σ_8 inferred from larger structures, this would clearly hint at the presence of Early Dark Energy.

For a given σ_8 measured from linear fluctuations, the Early Dark Energy models predict a substantially slower evolution of the halo population as in the ΛCDM model. This prediction has several immediate observable consequences. First, the evolution of the X-ray cluster luminosity function towards redshift unity should be somewhat flatter than expected in a ΛCDM universe. Current data are probably still insufficient for quantitative tests. Second, the dynamical activity of clusters near redshift unity should be substantially higher than expected in ΛCDM. The number of major mergers experienced by cluster-sized halos near redshift unity is predicted to be ~ 5 times higher than

in ΛCDM. Third, and most prominently, the number of clusters expected to be found in thermal Sunyaev-Zel'dovich surveys should increase substantially. Applying a simple model for cluster detection by the *Planck* satellite, we found that ~ 2 times more clusters should be found at arbitrary redshifts by *Planck* than in a ΛCDM universe, but ~ 10 times more above redshift unity. Leaving the question aside of how redshifts could be measured for clusters detected exclusively by their thermal Sunyaev-Zel'dovich effect, this prediction will be testable very soon. We note that this consequence of Early Dark Energy may naturally explain the high fluctuation amplitude of CMB temperature fluctuations on arc-minute scales, the so-called "CBI anomaly" (Padin et al., 2001; Mason et al., 2003; Bond et al., 2005).

Given these results, we arrive at the main conclusion that models for Early Dark Energy will leave a measurable imprint on weak-lensing measurements and determinations of the distance-redshift relation which is measured using type-Ia supernovae, but their most distinguishing signature is the slow evolution of the cluster abundance between redshifts ~ 1 and zero. Structure formation being hierarchical, this also implies a similar effect on the abundance evolution of galaxy-sized halos at substantially higher redshifts, $z \gtrsim 2 - 3$.

A

REFERENCES

Bartelmann, M., Meneghetti, M., Perrotta, F., Baccigalupi, C., & Moscardini, L. 2003, A&A, 409, 449
Bartelmann, M., Perrotta, F., & Baccigalupi, C. 2002, A&A, 396, 21
Bartelmann, M. & Schneider, P. 2001, Physics Reports, 340, 291
Bond, J., Cole, S., Efstathiou, G., & Kaiser, N. 1991, ApJ, 379, 440
Bond, J., Contaldi, C., Pen, U.-L., et al. 2005, ApJ, 626, 12
Bullock, J., Kolatt, T., Sigad, Y., et al. 2001, MNRAS, 321, 559
Caldwell, R. 2002, Physics Letters B, 545, 23
Caldwell, R., Dave, R., & Steinhardt, P. 1998, Physical Review Letters, 80, 1582
Caldwell, R., Doran, M., Müller, C., Schäfer, G., & Wetterich, C. 2003, ApJL, 591, L75
da Silva, A., Barbosa, D., Liddle, A., & Thomas, P. 2000, MNRAS, 317, 37
Dolag, K., Bartelmann, M., Perrotta, F., Baccigalupi, C., et al. 2004, A&A, 416, 853
Doran, M. & Jäckel, J. 2002, PRD, 66, 043519
Doran, M., Lilley, M., Schwindt, J., & Wetterich, C. 2001a, ApJ, 559, 501
Doran, M., Schwindt, J., & Wetterich, C. 2001b, Phys. Rev. D, 64, 123520
Eke, V., Navarro, J., & Steinmetz, M. 2001, ApJ, 554, 114
Ferreira, P. & Joyce, M. 1998, PRD, 58, 023503
Goldstein, J., Ade, P., Bock, J., et al. 2003, ApJ, 599, 773
Hawkins, E., Maddox, S., Cole, S., Lahav, O., et al. 2003, MNRAS, 346, 78
Horellou, C. & Berge, J. 2005, MNRAS, 360, 1393
Kitayama, T. & Suto, Y. 1996, ApJ, 469, 480
Klypin, A., Macciò, A., Mainini, R., & Bonometto, S. 2003, ApJ, 599, 31
Lacey, C. & Cole, S. 1993, MNRAS, 262, 627
Lacey, C. & Cole, S. 1994, MNRAS, 271, 676
Lahav, O., Lilje, P., Primack, J., & Rees, M. 1991, MNRAS, 251, 128
Liddle, A. & Scherrer, R. 1999, PRD, 59, 023509
Linder, E. & Jenkins, A. 2003, MNRAS, 346, 573
Ma, C., Caldwell, R., Bode, P., & Wang, L. 1999, ApJL, 521, L1
Maor, I. & Lahav, O. 2005, ArXiv Astrophysics e-prints; arXiv:astro-ph/0505308
Mason, B., Pearson, T., Readhead, A., et al. 2003, ApJ, 591, 540
Meneghetti, M., Bartelmann, M., Dolag, K., et al. 2004, A&A, submitted; preprint astro-ph/0405070
Navarro, J., Frenk, C., & White, S. 1997, ApJ, 490, 493
Padin, S., Cartwright, J., Mason, B., et al. 2001, ApJL, 549, L1
Power, C., Navarro, J., Jenkins, A., et al. 2003, MNRAS, 338, 14
Press, W. & Schechter, P. 1974, ApJ, 187, 425
Ratra, B. & Peebles, P. 1988, PRD, 37, 3406
Readhead, A., Mason, B., Contaldi, C., et al. 2004, ApJ, 609, 498
Rebolo, R., Battye, R., Carreira, P., et al. 2004, MNRAS, 353, 747
Riess, A., Strolger, L.-G., Tonry, J., Casertano, S., et al. 2004, ApJ, 607, 665
Schäfer, B. M., Pfrommer, C., Hell, R., & Bartelmann, M. 2004, ArXiv Astrophysics e-prints; astro-ph/0407090
Schneider, P., Ehlers, J., & Falco, E. E. 1992, Gravitational Lenses (Springer Verlag, Heidelberg)
Sheth, R. & Tormen, G. 1999, MNRAS, 308, 119
Spergel, D., Verde, L., Peiris, H., Komatsu, E., et al. 2003, ApJS, 148, 175
Sunyaev, R. & Zeldovich, Y. 1972, Comments on Astrophysics and Space Physics, 4, 173
Tegmark, M., Strauss, M., Blanton, M., Abazajian, S., et al. 2004, PRD, 69, 103501
Wang, L. & Steinhardt, P. 1998, ApJ, 508, 483
Weinberg, N. & Kamionkowski, M. 2003, MNRAS, 341, 251
Wetterich, C. 1988, Nuclear Physics B, 302, 668
Wetterich, C. 2004, Physics Letters B, 594, 17
Zlatev, I. & Steinhardt, P. 1999, Physics Letters B, 459, 570

A. T

The conventional calculation used in many papers (see, e.g. Lahav et al. 1991; Kitayama & Suto 1996; Wang & Steinhardt 1998; Weinberg & Kamionkowski 2003; Horellou & Berge 2005; Maor & Lahav 2005) starts from the Friedmann equation (4) for the second time derivative $\ddot{y}$ of the perturbation radius and converts it to an energy equation after multiplication with $\dot{y}$. This energy equation contains the cosmological constant or Dark-Energy density in a term which appears analogous to a potential-energy term. Energy conservation is then used by equating the total potential energy of the overdense sphere at turn-around to the sum of kinetic and potential energies at virialisation, which can be expressed solely in terms of the potential energy by means of the virial theorem.

Following this approach, assuming that the Dark Energy does not clump and therefore not participate either in the virialisation of the collapsing overdensity (see Maor & Lahav (2005) for a thorough discussion), we calculate Δ_v and confirm that it is only weakly modified by Early Dark Energy compared to, e.g. the ΛCDM result.

We show in Fig. 12 the virial overdensity Δ_v calculated in this way as a function of the collapse redshift z_c for two models of Early Dark Energy and compare it to the results for a ΛCDM with $\Omega_{m,0} = 0.3$ and $\Omega_{\Lambda,0} = 0.7$, and an OCDM model with $\Omega_{m,0} = 0.3$. While Δ_v is somewhat lower at moderate and high z_c for the Early-DE models than for ΛCDM, the difference between them remains moderate. For high z_c, they approach the "canonical" value of $18\pi^2 \approx 178$ and fall towards $\Delta_v \approx 110$ for $z_c = 0$. As shown for comparison, Δ_v shows a substantially flatter behaviour with z_c in the OCDM model.
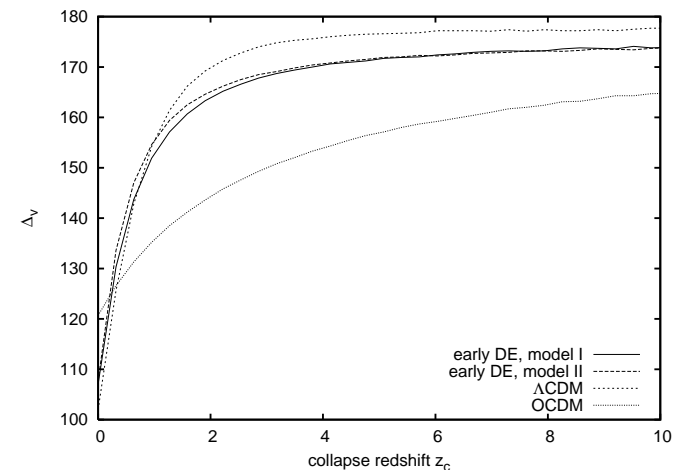

F . 12.—The virial overdensity Δ_v is shown as a function of collapse redshift z_c for the same four cosmologies used in Fig. 1. The change in Δ_v due to Early Dark Energy is small compared to the difference between the more conventional models.

We have, however, serious doubts about whether this approach is valid in the context of cosmological models with (Early) Dark Energy. The virial theorem concerns time-averaged

energies of particles in bound orbits. Dark-matter particles orbiting within collapsing overdensities, however, will not feel any force from the Dark Energy because the latter is homogeneously distributed. Thus, it appears dubious to assign a potential to the Dark Energy whose gradient should appear as a conservative force term in the equation of motion. Rather, the Dark Energy should only appear acting on the expansion of the background, and therefore as a dissipative force term which should time-average out of the virial theorem. In this picture, the concept of energy conservation also needs to be revisited. Since none of our later results depends on Δ_v, we leave the discussion at that point, showing Δ_v as the conventional approach predicts it for the Early Dark-Energy models, but expressing qualms regarding the validity of the underlying physical concepts.